Research Square

Preprints are preliminary reports that have not undergone peer review.
They should not be considered conclusive, used to inform clinical practice,
or referenced by the media as validated information.

Fabrication and Electrical Characterization of Radio Frequency Magnetron Sputtered Al_2O_3 Thin-Film Metal–Insulator–Metal Capacitors on Platinized Silicon

Abdullah

p22ee001@iitj.ac.in

Indian Institute of Technology Jodhpur https://orcid.org/0000-0001-9487-2595

Research Article

Keywords: Al_2O_3 thin films, RF magnetron sputtering, Metal–insulator–metal (MIM) capacitors, Platinized silicon, Leakage current density, Capacitance–voltage (C–V) characteristics, Conductance–voltage (G–V) characteristics, Dielectric constant, Frequency-dependent dielectric properties, High-dielectric materials

Posted Date: July 10th, 2026

DOI: https://doi.org/10.21203/rs.3.rs-10296245/v1

License: This work is licensed under a Creative Commons Attribution 4.0 International License.
Read Full License

Additional Declarations: The authors declare no competing interests.

Abstract

Capacitors based on high-k dielectric metal-insulator-metal (MIM) structures have been studied intensely recently because of their good insulator characteristics and constant performance. The study presented here involves fabrication of 60 nm thick Al_2O_3 thin films using radio frequency (RF) magnetron sputtering at room temperature on platinized silicon substrates and development of MIM capacitors with $Pt/Al_2O_3/Cr/Au$ multilayer structure. First of all, prior to film growth, the substrates were cleaned by the method of RCA cleaning. Then, the deposited films were examined using optical microscopy and atomic force microscopy (AFM). AFM showed that the films had smooth surface morphology with RMS roughness value of around 4.006 nm. Afterwards, circular Cr/Au (40/250 nm) top electrodes of diameter 500 μm were fabricated by thermal evaporation through shadow mask. Finally, leakage current density, capacitance-voltage (C-V) and conductance-voltage (G-V) measurements were performed at Keithley characterization station within the ranges of voltages ± 2 V, ± 3 V and ± 5 V at the frequencies 5 kHz – 1 MHz. The manufactured capacitors displayed negligible leakage current density and constant dielectric properties within the studied bias range. The capacitance demonstrated weak dependence on the applied voltage but depended on the frequency, thus causing a decrease in the capacitance density and estimated dielectric constant with an increase in frequency. The dielectric constant varied between 21 at 5 kHz and 12 at 1 MHz; the loss tangent was less than 0.06 within the studied frequency range. The presented results prove that the thin films produced by RF sputtering have stable dielectric properties and can be successfully utilized for the production of MIM capacitors.

Introduction

Metal-insulator-metal (MIM) capacitors are essential components of today's microelectronics industry, being used widely in analog/mixed signal ICs, RF devices, dynamic memories, sensors, and energy storage devices. With continuous miniaturization of electronic systems, there has been an increasing need for dielectrics that can offer not only a large capacitance density but also low leakage current, thermal stability, and high reliability [1]. Among several dielectric materials available, aluminum oxide (Al_2O_3) has drawn a lot of attention owing to its wide band gap, high dielectric strength, good chemical stability, compatibility with semiconductor technology processes, and low leakage current. Thin films made from aluminum oxide (Al_2O_3) have been applied in metal insulator metal (MIM) capacitors, metal-oxide-semiconductor (MOS) devices, thin-film transistors, resistive memories, and sensor platforms. Electrical properties of Al_2O_3 thin films largely depend on their preparation method, thickness, interfaces, defects, and microstructure [2]. A number of deposition techniques such as atomic layer deposition (ALD), chemical vapor deposition, pulsed laser deposition, solution-based processing, and RF magnetron sputtering have been applied for synthesizing Al_2O_3. Recent research works have extensively utilized multi-layered dielectrics by ALD, bilayers of Al_2O_3/HfO_2, nanolaminates of Al_2O_3/TiO_2, and superlattices for increasing dielectric constant and reducing leakage current. Simultaneously, studies on metal oxide semiconductor capacitors and dielectric layers reveal the significance of interface properties, defects, and charge traps on frequency-dependent electrical response [3, 4, 2]. However, little has been done in the field of investigation of single-layer RF-sputtered alumina-based MIM capacitors manufactured on

platinized silicon substrates from the standpoint of morphological and electrical properties analysis [5]. Roughness and structure of the surface may play a crucial role in leakage channels formation and dielectric response, whereas capacitance at different frequencies gives us additional details about polarization mechanisms, interface defects, and dielectric behavior. Thus, the study incorporating AFM measurements, optical microscopy, leakage current measurements, and capacitance analysis might be beneficial in characterizing the actual properties of the investigated material [6–7]. In this study, about 60 nm thickness Al2O3 thin films were deposited by radio frequency magnetron sputtering onto platinized Si substrates, where the fabrication of Au top circular electrodes via thermal evaporation technique through shadow mask was employed to develop the MIM capacitors [8]. The AFM analysis was done for the surface morphology of deposited thin films while the optical microscope analysis was done for both thin films and fabricated devices. Leakage current and capacitance as a function of frequency were measured as part of electrical characteristics. Capacitance density and effective dielectric constant were also calculated and discussed for the suitability of sputtered Al2O3 thin films as dielectrics and capacitors [9].

Literature Gap

The recent developments made in high-k dielectrics have facilitated a remarkable development in the design of MIM capacitors for ICs, radiofrequency (RF) circuits, memory cells, and sensors [1, 10]. The majority of published works are concentrated on ALD-deposited Al_2O_3 multilayer systems, nanolaminate structures, and bilayered dielectrics, like Al_2O_3/HfO_2 and Al_2O_3/TiO_2, in order to increase the value of dielectric constant, leakage current, and performance of capacitors. However, other researchers have studied the possibility to employ MOS capacitors, memristors, or complex interfaces using different fabrication approaches. Although such works can give some information on dielectrics properties and mechanisms of charge carriers transport, there are very few reports devoted to investigation of single-layer RF-deposited Al_2O_3 MIM capacitors on platinumized silicon with Au top electrode [11–12]. Also, even though surface morphology, leakage currents, and capacitance properties have been separately studied in some researches, an analysis correlating surface morphology by means of AFM, optical properties, leakage current behavior, and capacitance behavior in dependence on frequency of the sputtered Al_2O_3 MIM structure have not been sufficiently studied yet [13, 14]. Additionally, a complete evaluation of capacitance across wide ranges of frequencies along with some additional parameters including the capacitance density and dielectric constant has not been widely presented for the simple sputtered Al_2O_3 dielectrics. It means that an experimental study correlating all these factors is necessary to be done [15, 16]. In this research, an experimental study of single-layer RF-sputtered aluminum oxide MIM capacitors through correlation of AFM measurements of surface morphology and frequency response of their capacitive and leakage currents is conducted to evaluate dielectric quality employing a straightforward method for fabrication of devices under consideration [17, 18]. Unlike plenty of studies on multilayer dielectric systems and MOS structures fabricated employing ALD technique, there is a lack of comprehensive investigations of structural and frequency-dependent electrical properties of single-layer RF-sputtered aluminum oxide MIM capacitors on platinized silicon substrates [19, 20].

Experimental

2.1 Substrate Preparation

Platinized silicon substrates purchased commercially were employed as the bottom electrode substrate for the MIM capacitor preparation process [21, 22]. The substrate comprised a silicon wafer having a 5000 Å thickness of SiO_2 deposited on its surface, followed by 400 Å of Ti (or TiO_2 where required) adhesion layer and a 2000 Å thickness of platinum as the bottom electrode. Before the deposition of thin films, the substrates were carefully cleaned through the standard RCA-1 and RCA-2 methods to remove any organic, metallic particles, and other contaminations from the substrates [23, 24, 25].

2.2 Al_2O_3 Thin-Film Deposition

Following the RCA cleaning procedure, a thin film of Al_2O_3 dielectric was sputtered on the platinized silicon substrates using a radiofrequency (RF) magnetron sputtering technique. An Al_2O_3 sputter target with a diameter of 2 inches was used in this experiment [26, 27]. RF sputtering was done at the standard operating frequency of 13.56 MHz with an input power of 100 Watts. In preparation for deposition, the sputtering chamber was first evacuated to achieve a base pressure of 2×10^{-6} mbar. The deposition of the film was then carried out using argon (Ar) gas at a working pressure of 5.3×10^{-3} mbar and at a gas flow rate of 40 SCCM [28].

Substrate heating was not deliberately applied during deposition but rather was carried out at room temperature (RT) and while rotating the substrates for better deposition uniformity [29]. The duration of the deposition process was 90 minutes, corresponding to an Al_2O_3 film thickness of 60 nm. The deposited Al_2O_3 dielectric film formed part of the MIM capacitor structure and was subsequently tested for morphology and electrical characteristics [30].

2.3 Surface Characterization and Top Electrode Fabrication

Prior to top electrode deposition, sputtered Al_2O_3 thin films were investigated for the surface quality and uniformity. In terms of macroscopic uniformity, optical microscope was used whereas atomic force microscopy (AFM) was employed for the investigation of surface morphology and quantification of roughness at the nanometer scale level [31].

For formation of top circular electrodes, thermal evaporation method through the use of shadow mask was adopted. For the formation of top circular electrodes, 10 nm thick Cr layer and 200 nm thick Au layer were deposited. In this regard, Cr layer acted as the adhesive layer while Au was used as conductive electrode [32–33]. Formation of circular electrodes resulted in an overall size of 500 µm. It should be noted that the center-to-center spacing between two consecutive circular electrodes was 600 µm [34, 35].

2.4 Electrical Characterization

The electrical properties of the produced $Pt/Al_2O_3/Cr/Au$ MIM capacitors were characterized through C–V analysis and leakage current measurements. The frequency dependence of the C–V profile was obtained by means of a Keithley 4200B Semiconductor Characterization System with the CVU module in the designated ranges of frequency and bias voltage [36]. The leakage current was measured by means of a Keithley 2634B SourceMeter and calculated for the active area of the circular electrodes. The overall analysis of both the structural and electrical properties made possible an estimation of the dielectric and insulation performance of sputtered Al_2O_3 films [37, 38].

Optical micrographs of the RF magnetron sputtered Al_2O_3 thin film on the platinized silicon substrate are depicted in Fig. 1. As evident from Fig. 1a, it is clearly visible that there is a difference in the two regions, where one is the Al_2O_3 coated and other is an adjacent uncoated platinized silicon region. This indicates that there has been a successful deposition of the dielectric layer onto the desired substrate area [39]. It is seen that there are no apparent defects present in the coated layer, and the film is continuously covering the substrate. Figure 1b shows that the surface of the coating is very homogenous, and there is no sign of cracking, agglomeration, or peeling out of the thin film [40, 41].

From the AFM study, there was relatively consistent surface morphology exhibited by the thin film of Al_2O_3 grown using RF sputtering technique, with the average surface roughness value being 4.006 nm [42].

The figure below (Fig. 3) describes the design structure and the fabricated structure of the $Pt/Al_2O_3/Cr/Au$ metal-insulator-metal (MIM) capacitor. Figure 3a below depicts the structure design, which has been fabricated on platinized silicon substrate having the layer deposition structure as $Si/SiO_2/Ti/Pt$. On top of these layers, a 60 nm RF sputtering technique of the Al_2O_3 insulating layer has been made [43, 44]. The top circular Cr/Au electrodes have then been evaporated using thermal evaporation technique using a shadow mask to form the MIM capacitor structure. Figure 3b is the layout diagram of the device showing the arrangement of circular Cr/Au top electrodes employed for the measurement purposes. The fabricated device has been captured under an optical microscope as in Fig. 3c [45]

Result and Analysis

In Fig. 4, the graph depicts the relationship between the leakage current density (J) and the applied bias voltage for the MIM capacitor structures consisting of $Pt/Al_2O_3/Cr/Au$ fabricated using the three different ranges of applied voltage sweeps ranging from − 2V to +2V, -3V to +3V, and − 5V to +5V. As shown in the graph, the leakage current density rises as the applied voltage bias increases in all cases, which is because of the rise in electric field strength in the Al_2O_3 insulator layer [46]. Figure 4a shows the leakage current density of the device is quite low with respect to the ± 2 V range bias, where the value of the current density stays in the order of 10^{-7} A/cm². However, for ± 3 V sweep, illustrated in Fig. 4b, leakage current density increases but still remains within the same order of magnitude [47]. This can be explained by the increased electric field, which makes the movement of carriers within the insulation more likely. Lack of abrupt increase in current proves the fact that there was no breakage of dielectric

within the tested range [48, 9]. In case of the highest voltage range, which equals to ± 5 V (refer to Fig. 4c), we can observe the leakage current density, which gets close to the value of 10^{-6} A/cm². It is possible to explain such behavior by increased possibility of charge injection due to larger electric field, which leads to charge movement through the dielectric. However, despite the increase in leakage current, it stays rather stable at this range of voltages. All in all, the leakage current properties confirm that the aluminum oxide film fabricated via the RF-sputtering process at 60 nm shows consistent dielectric operation for a broad range of bias voltages [49]. The low leakage current value at low voltages and steady increase at high voltages show that the film has a high level of quality and leakage current suppression. This behavior is required for MIM capacitor devices. The rise in leakage current density under an increased voltage is due to charge transport mechanisms in the film influenced by high electric fields [50].

Figure 5 shows the dependence of the leakage current density (J) on the electric field (E) applied to the fabricated MIM capacitors of structure Pt/Al_2O_3/Cr/Au. The electric field values were obtained by applying different bias voltages to the capacitors according to the equation E = V/t, with t = 60 nm being the thickness of the deposited Al_2O_3 layer. The tests were carried out for ± 2 V, ± 3 V, and ± 5 V sweep ranges corresponding to the ranges presented in Fig. 5a, Fig. 5b, and Fig. 5c, respectively [51, 20]. It can be clearly seen that the dependence of leakage current density on the electric field is characterized by its increasing trend as the applied electric field is increased under all tested conditions. In case of relatively small values of applied field, leakage current density does not reach significant values due to the good insulation properties of the 60 nm thick layer of Al_2O_3 [52]. In the case of the ± 2 V sweep (see Fig. 5a), the electric field is approximately ± 0.33 MV/cm, while the obtained current density is still in the range of 10^{-7}A/cm², confirming the efficient operation of the dielectric insulation material at moderate voltage levels [53]. With the expansion of the sweep voltage to ± 3 V (see Fig. 5b), the value of the electric field is about ± 0.50 MV/cm, resulting in a moderate rise in leakage current density but maintaining the efficiency of the system operation. At the voltage sweep of ± 5 V (see Fig. 5c), where the electric field equals ± 0.83 MV/cm, the leakage current density achieves the value of around 10^{-6} A/cm² [54]. The continuous variation of current density with the electric field confirms that the deposited Al_2O_3 film has electrical insulating properties at all the measured bias voltages. The lack of breakdown behavior also supports that the sputtered dielectric layer has uniform properties [55]. It can be concluded from this experiment that the MIM capacitors manufactured using RF sputtering are highly stable at higher electric fields and exhibit no leakage behavior, hence making them suitable candidates for application as dielectric layers [56].

The variation in current density with respect to the electric field suggests field-enhanced charge conduction, possibly by defect-assisted conduction mechanisms, but determination of the conduction mechanism would need separate analysis [57].

Fg.7. Conductance–voltage (G–V) characteristics of the fabricated Pt/Al_2O_3/Cr/Au metal–insulator–metal (MIM) capacitors measured at frequencies of 5 kHz, 10 kHz, 50 kHz, 100 kHz, 500 kHz, and 1 MHz under different voltage sweep ranges: **(a)** − 2 V to + 2 V and **(b)** − 5 V to + 5 V.

The figure below (**Fig. 7**) represents the conductance-voltage (G-V) curves for the Pt/Al_2O_3/Cr/Au MIM capacitors fabricated with different frequencies of 5 kHz, 10 kHz, 50 kHz, 100 kHz, 500 kHz, and 1 MHz under sweep voltages of − 2 V to + 2 V and − 5 V to + 5 V. It can be seen from **Fig. 7a**, which represents the G-V curve for ± 2 V sweep, that the conductance shows a slightly parabolic nature depending upon the bias applied. Here, the conductance attains its minimum value when the voltage is zero and then rises linearly with both positive and negative bias, leading to symmetric nature of the curve [61]. It implies that the transport of charges across the dielectric layer is independent of the external electric field, and with increasing applied voltage, the effect of the field on conductivity becomes significant. It is evident that there is frequency dependence in the case of the measurements made using ± 2 V as well. There is a difference in the conductance values according to the measuring frequency. These are caused by changes in the AC behavior of the dielectric and its lossy behavior [62]. This is typically observed due to polarization effects and dielectric relaxation. On the other hand, the measurements carried out at ±5V shown in **Fig. 7b** reveal that the conductance values do not change over the range and that there are small fluctuations in them. In fact, these curves for different frequencies are distinguished from each other clearly and this shows that the dependence of the measured conductance is more on the excitation frequency rather than the bias voltage [63]. Generally speaking, the properties of G-V suggest that the RF-sputtered Al_2O_3 dielectric film with a thickness of 60 nm shows stable behavior in terms of conductance, low voltage dependency, and reliable frequency behavior. Considering the above-discussed features of C-V and leakage currents, one can conclude that the fabricated Pt/Al_2O_3/Cr/Au MIM capacitors feature good electrical properties. Specifically, the gradual decrease of conductance with increasing frequency suggests that the electrical properties of the device depend on dielectric relaxation and polarization effects but do not have sharp transitions, which can be attributed to shifts in conductivity mechanisms. The stability of G-V in both cases confirms the reliable insulating property of the Al_2O_3 film [64].

The dependence of capacitance density on the measurement frequency in the fabricated Pt/Al_2O_3/Cr/Au MIM capacitors in the voltage sweep range of − 2 V to + 2 V and − 5 V to + 5 V, respectively, is shown in Fig. 8. The calculation of capacitance density was carried out using the measurement value of the capacitance divided by the area of the top electrode [65]. In Fig. 8a shows that with regard to the voltage sweep of ± 2 V, the capacitance density shows a gradual drop from 0.31 μF/cm² at 5 kHz to 0.28 μF/cm² at 50–100 kHz. Afterwards, the capacitance density showed a sharp drop down to 0.18 μF/cm² at 1 MHz [66]. Similar results were obtained from Fig. 8b in which the voltage sweep of ± 5 V is considered. The decrease in the capacitance density value due to increasing frequency is in agreement with the results obtained through the C-V measurements due to the frequency dependence of the dielectric properties of the sputtered aluminum oxide layer. Under lower frequencies, slow polarization effects and localized charges could respond to the AC stimulation more effectively, and thus, there was an enhanced capacitance density. With increasing measurement frequency, this effect decreased progressively, causing a reduction in the overall capacitance and thus capacitance density [67]. It is worth noting that the capacitance density of fabricated MIM capacitors was quite unaffected by the magnitude of the applied DC voltage sweeps, as can be observed from both ± 2 V and ± 5 V experiments. In other words,

the measurement frequency has had a greater impact on the dielectric properties than the DC voltage in the analyzed range. In summary, the findings on frequency-dependent capacitance density prove that the Al_2O_3 thin film prepared by RF-sputtering has stable capacitor properties even in a wide range of frequencies, whereas the gradual decline in capacitance at high frequencies is typical for the dielectric dispersion phenomenon. The decrease in the capacitance density along with the decrease in the dielectric constant as the frequency increases implies that the frequency response characteristics of the MIM capacitors under study depend mostly on dielectric dispersion [68].

In Fig. 9 below, the variations of the estimated dielectric constant (k) and loss tangent (tan ∂) of the manufactured Pt/Al_2O_3/Cr/Au MIM capacitors with respect to the measurement frequency have been shown. These values were calculated based on the measured capacitance and conductance results for the voltage range of − 5 V to + 5 V [69]. From Fig. 9 above, it is evident that the dielectric constant reduces with an increase in measurement frequency, from around 21 for a measurement frequency of 5 kHz to approximately 12 for a measurement frequency of 1 MHz. It can be explained by the frequency dependence of the capacitance. With low measurement frequency, it allows more time for the polarization effects and localized charges to redistribute within the capacitor. Therefore, there will be higher dielectric constant estimation compared with those at high measurement frequency, which is beyond the reach of the slower polarization effect. On the contrary, the loss tangent (tan ∂) demonstrates a gradually increasing trend at a high frequency of around 0.036 for 5 kHz and 0.056 for 1 MHz [70]. The increment in loss tangent means that energy losses associated with dielectrics increase along with the increase in excitation frequency, which can be explained by the frequency-dependent AC characteristics of the prepared material. However, it should be emphasized that even the highest value of loss tangent does not exceed 0.06, which proves the stability of AC characteristics of the developed dielectric. The decreasing dielectric constant and increasing loss tangent are typical for dielectric dispersion, as can be concluded based on C–V and capacitance density dependencies. Overall, the results prove that the dielectric properties of the investigated material are stable in the analyzed range of excitation frequency but demonstrate expected changes connected to the reduction in polarization [71]. Generally, the obtained results concerning dielectric properties suggest the possibility of application of the fabricated Al_2O_3 thin film having a high dielectric constant value at low-frequency measurements along with acceptable dielectric losses in metal–insulator–metal capacitors.The frequency dependency of the calculated dielectric constant and loss tangent was estimated based on capacitance and parallel conductance values applying the standard equivalent circuit relations. Generally, the trends observed are associated mainly with dielectric dispersion effect [**72–73**]

Conclusion

The present work reported the successful fabrication of Pt/Al_2O_3/Cr/Au MIM capacitor structures with a dielectric layer of Al_2O_3 that is sputtered to a thickness of 60 nm on platinized silicon substrate after cleaning using the RCA method. Microscopic and AFM techniques verified that a thin film with an RMS surface roughness of about 4.006 nm was successfully formed. Circular Cr/Au top electrodes deposited by thermal evaporation process made it possible to perform the electrical tests of the devices. The

leakage current measurements were conducted at voltage sweeps of ± 2 V, ± 3 V, and ± 5 V and showed stable behavior of the film as an insulator with the increase in leakage current density under the increase in the electric field value without dielectric breakdown at the given experimental interval. The frequency dependency C–V measurements illustrated that capacitance did not depend significantly on the DC bias, while it decreased when increasing the measuring frequency due to the dielectric dispersion in the sputtered layer of aluminum oxide. In addition, a similar pattern was observed for capacitance density, whereas the dielectric constant decreased from about 21 at low frequencies to approximately 12 at 1 MHz. The loss tangent values were relatively low (less than 0.06). In summary, the obtained results confirm that RF magnetron sputtered Al_2O_3 films on platinized silicon possess appropriate insulating and capacitive properties due to their low loss tangent and leakage current, thus being promising materials for manufacturing integrated capacitors as well as other electronic components.

Declarations

Acknowledgement

The authors thank Prof. Mahesh Kumar and the Central Research Facility (CRF), IIT Jodhpur, for providing access to the facilities and instruments used in this research.

Conflict of interest.

The authors declare that they have no conflict of interest.

Data availability.

Data will be made available on request.

References

1. Cao B, Duan Y, Shao L (2026) Modeling and Characterization of Thin Al2O3–HfO2 Stacked Metal–Insulator–Metal and Deep Trench Decoupling Capacitors for Advanced Packaging Applications. J Phys : Conf Ser 3223:012011. https://doi.org/10.1088/1742-6596/3223/1/012011
2. Rocha-Aguilera D, Méndez-Jerónimo G, Molina-Reyes J (2026) Impact of Interface Properties on Direct Tunneling in Al/ALD-Al2O3/Al Capacitors for Josephson Junction Applications. IEEE Trans Quantum Eng. https://doi.org/10.1109/TQE.2026.3700568
3. Kang H, Yuan S, Wang Y, Zhang J, Zhao D, Chai Z, Lu X (2025) Effect of film thickness on solution-processed Al2O3 high-k dielectric properties and TFT performance. SSRN Preprint https://ssrn.com/abstract=6721622

4. Kastian DB, Bermundo JPS, Uraoka Y (2026) Influence of bilayer high-k Al2O3 and HfO2 gate insulators on the electrical performance of amorphous oxide thin-film transistors. J Phys D: Appl Phys 59:045102. https://doi.org/10.1088/1361-6463/ae357c
5. Padhi PS, Rai SK, Goutam UK, Ajimsha RS, Verma S, Misra P (2026) Effect of Continuous-to-Discontinuous Layer Transition on the Interface Evolution and Dielectric Response in Subnanometric Al2O3/TiO2 Laminates Grown by Atomic Layer Deposition. ACS Appl Mater Interfaces 18:32049–32063. https://doi.org/10.1021/acsami.6c05777
6. Xu Y, Pan Y, Gao L, Zhang F, Ma M, Liang J, Liu Z (2026) Compositional control and electrical performance of atomic layer deposited Al2O3/TiO2 nanolaminates. Mater Sci Semicond Process 201:110105. https://doi.org/10.1016/j.mssp.2025.110105
7. Lok R (2025) The Effects of Temperature and Frequency on the Electrical and Dielectric Properties of Al2O3 Structure. Silicon 17:2131–2142. https://doi.org/10.1007/s12633-025-03329-0
8. Fohn C, Zharfan F, Chery E, Croes K, Stucchi M, Afanas'ev V (2025) Impact of Al-doping on Al:HfO2 dielectric reliability in MIM capacitors, in: 2025 IEEE International Reliability Physics Symposium (IRPS), IEEE. https://doi.org/10.1109/IRPS48204.2025.10982827
9. Nepal M, Dhakal TP (2025) Oxidant-Dependent Conduction in Early-Cycle Atomic-Layer-Deposited Al2O3 and Its Impact on the Dielectric Behavior of Al2O3/TiO2 Nanolaminates. ACS Appl Mater Interfaces 17:68169–68178. https://doi.org/10.1021/acsami.5c18459
10. Bergman H (2025) Direct Current Leakage in CNF-MIM Capacitors with High-k Dielectric and TiN Electrode, Degree Project in Electrical Engineering. Chalmers University of Technology, Gothenburg, Sweden
11. Mousavi Karimi Z, Davis JA (2025) Enhanced Permittivity in PEALD Al2O3/TiO2 Nanolaminates: Investigating Maxwell-Wagner and Interfacial Polarization in IDEs, in: 2025 IEEE 37th International Conference on Microelectronic Test Structures (ICMTS), IEEE. https://doi.org/10.1109/ICMTS63811.2025.11068916
12. Saro S, Palestri P, Caruso E, Toniutti P, Driussi F (Jan. 2026) Dielectric Absorption Caused by Traps in MIM/MOS Capacitors: A New Model Validated Through TCAD. IEEE Trans Electron Devices 73(1):20–26. https://doi.org/10.1109/TED.2025.3633623
13. Kastian DB, Bermundo JPS, Uraoka Y (2026) Influence of bilayer high-k Al2O3 and HfO2 gate insulators on the electrical performance of amorphous oxide thin-film transistors. J Phys D 59:045102. https://doi.org/10.1088/1361-6463/ae357c
14. Xu Y, Pan Y, Gao L, Zhang F, Ma M, Liang J, Liu Z (2026) Compositional control and electrical performance of atomic layer deposited Al2O3/TiO2 nanolaminates, Materials Science in Semiconductor Processing, vol. 201, Art. 110105. https://doi.org/10.1016/j.mssp.2025.110105
15. Meza-Arroyo J, Dunna B, Xu W, Chen Y-C, Chen J-S, Hsu JWP (2026) Bayesian Optimization of Multi-Bit Pulse Encoding in In_2O_3/Al_2O_3. Thin-Film Transistors for Temporal Data Processing, preprint/manuscript

16. Padhi PS, Rai SK, Goutam UK, Ajimsha RS, Verma S, Misra P (2026) Effect of Continuous-to-Discontinuous Layer Transition on the Interface Evolution and Dielectric Response in Subnanometric Al_2O_3/TiO_2 Laminates Grown by Atomic Layer Deposition. ACS Appl Mater Interfaces 18:32049–32063. https://doi.org/10.1021/acsami.6c05777
17. Seibertz BBO, Szyszka B (2025) Deposition of High-k Tantalum Oxide by DC Hollow Cathode Gas Flow Sputtering and the Influence of DC and Pulsed DC Substrate Bias. IEEE J Electron Devices Soc 13. https://doi.org/10.1109/JEDS.2025.3624015
18. Yang C-M, Yang Y-C, Tsui LS, Satheesh A, Jiang B-H, Chen C-P (Oct. 2025) Improvements in the Stability and Photocurrent of Organic-Semiconductor-Based Light-Addressable Potentiometric Sensors via ALD Stacked Sensing Membranes and Electron Transport Layers. IEEE Sens J 25(20):37674–37682. https://doi.org/10.1109/JSEN.2025.3602998
19. Kumar S, Yadav D, Ramesh R, Stathopoulos S, Tsiamis A, Prodromakis T (Apr. 2025) Electrical Analysis of Atomic Layer Deposited Thin HfO_2 and HfO_2/Ta_2O_5-Based Memristive Devices. IEEE Trans Electron Devices 72(4):1780–1787. https://doi.org/10.1109/TED.2025.3539256
20. Xiong L, Hu J, Yang Z, Li X, Zhang H, Zhang G (2022) Dielectric Properties Investigation of Metal–Insulator–Metal (MIM) Capacitors, Molecules, vol. 27, no. 12, Art. 3951. https://doi.org/10.3390/molecules27123951
21. Lok R (2025) The Effects of Temperature and Frequency on the Electrical and Dielectric Properties of Al2O3 Structure. Silicon 17:2131–2142. https://doi.org/10.1007/s12633-025-03329-0
22. Kannadassan D, Sivasankaran K, Kumaravel S, Cheng C-H, Shojaei Baghini M, Mallick PS (2024) High-k Metal–Insulator–Metal Capacitors for RF and Mixed-Signal VLSI Circuits: Challenges and Opportunities, Proceedings of the IEEE, vol. 112, no. 10, pp. 1610–1631. https://doi.org/10.1109/JPROC.2024.3506996
23. Mukhopadhyay P, Fletcher I, Couvertier ZC, Morris J, Perez J, Nichols C, Allgair J, Vandevere J, Schoenfeld WV, Aoki S, Novoselic E, Lombardo S, Triyoso D, Kretzschmar J, deVilliers A, Fulford J (Mar. 2024) High-Performance HfO2/Al2O3 Superlattice MIM Capacitor in a 200 mm High-Volume Batch-ALD Platform. IEEE Trans Electron Devices 71(3):2036–2042. https://doi.org/10.1109/TED.2024.3353702
24. Padhi PS, Ajimsha RS, Rai SK, Bose A, Misra P (2023) Effect of Al2O3 Layer Thickness on Leakage Current and Dielectric Properties of Atomic Layer Deposited Al2O3/TiO2/Al2O3 Nano-Stack, Journal of Materials Science: Materials in Electronics, vol. 34, art. 1160. https://doi.org/10.1007/s10854-023-10615-3
25. Fohn C, Zharfan F, Chery E, Croes K, Stucchi M, Afanas'ev V (2025) Impact of Al-Doping on Al:HfO2 Dielectric Reliability in MIM Capacitors, in *Proceedings of the 2025 IEEE International Reliability Physics Symposium (IRPS)*, https://doi.org/10.1109/IRPS48204.2025.10982827
26. Cho E, Kim MJ, Oh S, Park W, Yoon J, Cho B (2025) Enhancing Device Reliability in Pt/Ti/Al2O3/p-Ge Metal-Oxide-Semiconductor Memcapacitor via CF4 Plasma Treatment of Ge, Materials Science in Semiconductor Processing, vol. 194, art. 109576. https://doi.org/10.1016/j.mssp.2025.109576

27. Kwon O, Lee DH, Oh S, Yoon J, Kim H-B, Ahn J-H, Park W, Kim HS, Cho B (2026) Dynamic Control of Synaptic Plasticity by Competing Ferroelectric and Trap-Assisted Switching in IGZO Transistors with Al2O3/HfO2 Dielectrics. *Advanced Funct Materials* 36:e13449. https://doi.org/10.1002/adfm.202513449
28. Leon-Chaparro D, Englezos C, Mei B, Mul G, Katsoukis G (2026) Molecularly Modified Ultrathin Al2O3 Layers as Proton-Conductive, Oxygen-Impermeable Nanomembranes for Catalytic Surfaces. *Nanoscale* 18:6894–6905. https://doi.org/10.1039/D5NR04262C
29. Sun C, Yi T, Shi X, Dong J, Zhou Z, Han D, Zhang X (2026) A Ti/ITO Bilayer Gate Electrode Strategy for Improving Subthreshold Swing of Oxide Transistors. *Integrated Circuits Systems* early access. https://doi.org/10.23919/ICS.2026.3669096
30. Kwon O, Lee DH, Oh S, Yoon J, Kim H-B, Ahn J-H, Park W, Kim HS, Cho B (2026) Dynamic control of synaptic plasticity by competing ferroelectric and trap-assisted switching in IGZO transistors with Al2O3/HfO2 dielectrics. Adv Funct Mater 36:e202513449. https://doi.org/10.1002/adfm.202513449
31. Hasan ASMK, Islam MM, Mantooth HA (2025) Breakdown and C-V characteristics analysis of depletion mode lateral β-Ga2O3 MOSFET, in: Proc. 2025 International Compact Modeling Conference (ICMC), IEEE. https://doi.org/10.1109/ICMC64879.2025.11102334
32. Argenton P, Kah M, Eon D, Pernot J (2026) Comprehensive electrical analysis of interface states in Al2O3/OH-terminated (111) diamond MOSCap. Diam Relat Mater 161:113208. https://doi.org/10.1016/j.diamond.2025.113208
33. Liu J, Teraji T, Da B, Koide Y (2023) Electrical properties of boron-doped diamond MOSFETs with ozone as oxygen precursor for Al2O3 deposition. IEEE Trans Electron Devices 70(5):2199–2205. https://doi.org/10.1109/TED.2023.3256349
34. Manikanthababu N, Prajna K, Vas JV, Nguyen HPT (2026) Temperature-dependent conduction and dielectric engineering of dual-barrier Pt/PtOx/Nb2O5/SiO2/β-Ga2O3 MOS capacitors. IEEE Trans Electron Devices 73(5):2540–2546. https://doi.org/10.1109/TED.2026.3672411
35. Jia Y, Xiao T, Wang Z, Liu X, Wan H, Lu Q, Wang S, Chen H (2026) Influence of annealing temperature on the dielectric properties of (Al2O3)x(HfO2)(1 – x). J Mater Sci : Mater Electron 37:1214. https://doi.org/10.1007/s10854-026-17646-6
36. Argenton P, Kah M, Eon D, Pernot J (2026) Comprehensive electrical analysis of interface states in Al2O3/OH-terminated (111) diamond MOSCap. Diam Relat Mater 161:113208. https://doi.org/10.1016/j.diamond.2025.113208
37. Sun C, Yi T, Shi X, Dong J, Zhou Z, Han D, Zhang X (2026) A Ti/ITO bilayer gate electrode strategy for improving subthreshold swing of oxide transistors. Integr Circuits Syst. https://doi.org/10.23919/ICS.2026.3669096
38. Song C, Bu Y, Fang C, Wu F, Jiang X (2026) Precision etching process optimization and mechanism investigation for ultrathin Al2O3 thin films at the bottom of trenches. Appl Surf Sci 737:166861. https://doi.org/10.1016/j.apsusc.2026.166861

39. Dai P, Song J, Dong C, Gao Z, Zhang J, Wang Y, Zhang J, Li Y, Xin Q, Song A (2026) Oxygen-source-driven dielectric and interface engineering of ALD Al2O3 for high-performance and stable p-type SnO thin-film transistors. Appl Surf Sci 738:166950. https://doi.org/10.1016/j.apsusc.2026.166950
40. Varsha A, Jeyadheepan K, Subramanian B (2026) Interfacial charge modulation in sputtered CuO-Al2O3 bilayer thin films for enhanced formaldehyde sensing. Appl Surf Sci 742:167273. https://doi.org/10.1016/j.apsusc.2026.167273
41. Liang Z, Wu W, Fu X, Cai W, Ning H, Zheng H, He H, Su G, Yao R, Peng J (2026) Construction of high mobility and high stability rare earth semiconductor heterolayers by co-sputtering and co-doping for thin film transistor applications. J Alloys Compd 1071:188721. https://doi.org/10.1016/j.jallcom.2026.188721
42. Behera S, Panda CK, Lee S, Kim I, Lee H-J, Hwang J, Yoon S-G, Kim DW, Jang SC, Hong W, Jung J-W, Kim H-S (2025) Pioneering energy storage using facing-target sputtered Al2O3 protection layer on Ni-rich NCM622 cathode for high-efficiency all-solid-state thin-film batteries. Chem Eng J 522:167123. https://doi.org/10.1016/j.cej.2025.167123
43. Zhang X-Y, Peng D-C, Yan J-H, Zhang Z-X, Ruan Y-J, Zuo J, Xie A, Wu W-Y, Wuu D-S, Huang C-J, Lai F-M, Lien S-Y, Zhu W-Z (2023) Plasma power effect on crystallinity and density of AlN films deposited by plasma enhanced atomic layer deposition. J Mater Res Technol 27:4213–4223. https://doi.org/10.1016/j.jmrt.2023.10.302
44. Malik N, Gupta D, Kumar A, Singhal R, Kumar S, Aggarwal S (2025) Effect of post-annealing temperature and thickness on RF sputtered Al2O3 films for optoelectronic applications. Results Surf Interfaces 19:100480. https://doi.org/10.1016/j.rsurfi.2025.100480
45. Mariello M (2026) Microfabricated Neural Biosensors for Detection of Neurotransmitters, Biomarkers, and Small Molecules: Emerging Trends on Self-Sustained Systems and Energy Harvesting. Adv Sens Res 5:e00111. https://doi.org/10.1002/adsr.202500111
46. Li J, Li Z, Dong Q, Yu S (2026) Al2O3/Cu nanowire/Al2O3 sandwich architecture for high-performance flexible transparent conductive thin films. J Mater Sci: Mater Electron 37:355. https://doi.org/10.1007/s10854-026-16784-1
47. Sakka S (2022) History of ferroelectric materials prepared by sol-gel method. J Sol-Gel Sci Technol 101:140–175. https://doi.org/10.1007/s10971-021-05712-w
48. Pan F, Zhang F, Zhang H, Wang F, Wang L, Fu J, Yin F (2026) Microstructure, Mechanical Properties, and Corrosion Resistance of Al2O3/AlCoCrFeNi Nano-Multilayer Films Subjected to Post-Annealing. J Mater Eng Perform. https://doi.org/10.1007/s11665-026-14090-9
49. Jia Y, Fu Y, Liu X, Wang Z, Jiang P, Lu Q, Wang S, Guan Y, Li L, Chen H, Hao Y (2025) Different temperatures leakage mechanisms of (Al2O3)x(HfO2)1 – x gate dielectrics deposited by atomic layer deposition. Sci Rep 15:1154. https://doi.org/10.1038/s41598-025-85686-9
50. Pan F, Zhang F, Zhang H, Wang F, Wang L, Fu J, Yin F (2026) Microstructure, Mechanical Properties, and Corrosion Resistance of Al2O3/AlCoCrFeNi Nano-Multilayer Films Subjected to Post-Annealing. J Mater Eng Perform. https://doi.org/10.1007/s11665-026-14090-9

51. Bharti R, Mursaleen M, Dey A (2026) Tailoring multispectral infrared camouflage via vacuum-annealed Ag + TiN/TiN/Al_2O_3 thin films. Can Metall Q. https://doi.org/10.1080/00084433.2026.2684868
52. Jia Y, Xiao T, Wang Z, Liu X, Wan H, Lu Q, Wang S, Chen H (2026) Influence of annealing temperature on the dielectric properties of (Al2O3)x(HfO2)(1 – x). J Mater Sci : Mater Electron 37:1214. https://doi.org/10.1007/s10854-026-17646-6
53. Manchineni HV, Wachowiak A, Mikolajick T (2026) Impact of ALD Oxidant and Deposition Temperature on Electrical Characteristics of Al2O3/SiO2/SiC MOS-Capacitors. Mater Sci Forum 1192:21–28. https://doi.org/10.4028/p-0EmUTi
54. Xu Y, Pan Y, Gao L, Zhang F, Ma M, Liang J, Liu Z (2026) Compositional control and electrical performance of atomic layer deposited Al2O3/TiO2 nanolaminates. Mater Sci Semicond Process 201:110105. https://doi.org/10.1016/j.mssp.2025.110105
55. Deng W, Jiang M, Meng L, Feng J, Zhang J (2026) Significantly Enhanced High-Temperature Energy Storage Properties of Poly(ether imide) Dielectrics Enabled by Ultralow Content of Ni@Al2O3 Nanofibers. ACS Appl Mater Interfaces. https://doi.org/10.1021/acsami.6c05020
56. Gonçalez Filho W, Borga M, Geens K, Khan MA, Cingu D, Chatterjee U, Decoutere S, Knaepen W, Kizir S, Arnou P, Bakeroot B (2026) Poole–Frenkel Emission and Bulk Charge Trapping in AlON Deposited on GaN and Comparison to Al2O3. J Appl Phys 139:024101. https://doi.org/10.1063/5.0281468
57. Jia Y, Fu Y, Liu X, Wang Z, Jiang P, Lu Q, Wang S, Guan Y, Li L, Chen H, Hao Y (2025) Different Temperatures Leakage Mechanisms of (Al2O3)x(HfO2)1 – x Gate Dielectrics Deposited by Atomic Layer Deposition. Sci Rep 15:1154. https://doi.org/10.1038/s41598-025-85686-9
58. Jia Y, Xiao T, Wang Z, Liu X, Wan H, Lu Q, Wang S, Chen H (2026) Influence of annealing temperature on the dielectric properties of (Al2O3)x(HfO2)(1 – x). J Mater Sci: Mater Electron 37:1214. https://doi.org/10.1007/s10854-026-17646-6
59. Othmane DB (2025) Performance Enhancement of a-SiGe:H TFTs via SiO2/Al2O3 Bi-Layer Gate Dielectrics. Tech Phys 70(8):299–305. https://doi.org/10.1134/S1063784225600870
60. Jia Y, Fu Y, Liu X, Wang Z, Jiang P, Lu Q, Wang S, Guan Y, Li L, Chen H, Hao Y (2025) Different temperatures leakage mechanisms of (Al2O3)x(HfO2)1 – x gate dielectrics deposited by atomic layer deposition. Sci Rep 15:1154. https://doi.org/10.1038/s41598-025-85686-9
61. Pohekar P, Upadhyay BB, Parvez B, Ganguly S, Saha D (2025) Introduction of charge-trapping Al2O3/Ta2O5/Al2O3 dielectric stack in AlGaN/GaN high electron mobility transistors for programmable threshold voltage. Appl Phys Lett 126:112103. https://doi.org/10.1063/5.0243137
62. Xu Y, Pan Y, Gao L, Zhang F, Ma M, Liang J, Liu Z (2026) Compositional control and electrical performance of atomic layer deposited Al2O3/TiO2 nanolaminates. Mater Sci Semiconduct Process 201:110105. https://doi.org/10.1016/j.mssp.2025.110105
63. Deng W, Jiang M, Meng L, Feng J, Zhang J (2026) Significantly Enhanced High-Temperature Energy Storage Properties of Poly(ether imide) Dielectrics Enabled by Ultralow Content of Ni@Al2O3 Nanofibers. ACS Appl Mater Interfaces. https://doi.org/10.1021/acsami.6c05020

64. Huang X, Lv Q, Li Z, Zhao X, Liu S, Hou H, Liu G, Qiao G, Liu J (2026) Ultrathin Al2O3 interfacial engineering for high-performance self-powered Schottky photodetectors based on Cl-doped PbSe films. Infrared Phys Technol 156:106526. https://doi.org/10.1016/j.infrared.2026.106526
65. Zhang X, Xu Y, Duan J, Qu Z, Ji H, Ding C, Tian H, Gu J, Mitrovic I, van Zalinge H, Huang S, Zhang J, Li A, Liu W (2026) Monolithic Integrated GaN Complementary Logic Circuits Using AlON/Al2O3 Bilayer Gate Dielectric. IEEE Trans Electron Devices 73(6):3417–3424. https://doi.org/10.1109/TED.2026.3683046
66. Jha RK (2026) Tailoring crystallinity in Al2O3 dielectric films via PEALD and sputtering: Implications for thermal budget and device integration. MRS Adv. https://doi.org/10.1557/s43580-026-01654-z
67. Li J, Li Z, Dong Q, Yu S (2026) Al2O3/Cu nanowire/Al2O3 sandwich architecture for high-performance flexible transparent conductive thin films. J Mater Sci: Mater Electron 37:355. https://doi.org/10.1007/s10854-026-16784-1
68. Xiao N, Zhang H, Chen J, Tan H, Liu S, Zhu W, Wang X, Yu X, Xiao P, Chen D, Huang Y (2025) Application of high-k gate dielectric multilayer Al2O3/TiO2/Al2O3 anodized film in IGZO thin-film transistors. J Mater Sci: Mater Electron 36:1430. https://doi.org/10.1007/s10854-025-15496-2
69. Wagner LI, Streibel V, Luna E, Flashar KS, Anders W, Volkmer N, Steffen D, Munnik F, Zewdie TA, Santra S, Sharp ID, Yuan M (2025) Al1 – xHfxN Thin Films with Enhanced Piezoelectric Responses for GHz Surface Acoustic Wave Devices, arXiv arXiv:2511.18970. https://arxiv.org/abs/2511.18970
70. Park JH, He R, Hong IP, Kim MJ, Kim Y, Yu HK, Bark CW (2026) Synthesis of high-density Hf1 – xLaxO2 (HLO) ceramic targets with suppressed secondary phase and growth of thin films by rf magnetron sputtering. J Alloys Compd 1058:186958. https://doi.org/10.1016/j.jallcom.2026.186958
71. Hu D, Chen J, Su Z, Zhu W, Cai Q, Lao J, Wang X, Yu X, Xiao P (2023) Critical electric field stabilizing structure of Al2O3/TiO2/Al2O3 thin film for achieving high energy density. Ceram Int 49:17296–17304. https://doi.org/10.1016/j.ceramint.2023.02.096
72. Islam MM, Hasan MM, Ali A, Bae J, Jang J, Cost L (2022) Al2O3 and ZrAlOx Stack Passivation by Spray Pyrolysis for Highly Stable Amorphous InGaZnO Thin-Film Transistors. Adv Mater Interfaces 9:2200906. https://doi.org/10.1002/admi.202200906
73. Kumar K, Cahay M (2025) Low-temperature (< 300°C) crystalline Al2O3 thin film deposition by resistive thermal evaporation. J Vacuum Sci Technol B 43:032206. https://doi.org/10.1116/6.0004424
74. Schilirò E, Panasci SE, Mio AM, Nicotra G, Agnello S, Pécz B, Radnóczi GZ, Deretzis I, La Magna A, Roccaforte F, Lo Nigro R, Giannazzo F (2023) Direct atomic layer deposition of ultra-thin Al2O3 and HfO2 films on gold-supported monolayer MoS2. Appl Surf Sci 630:157476. https://doi.org/10.1016/j.apsusc.2023.157476

Figures

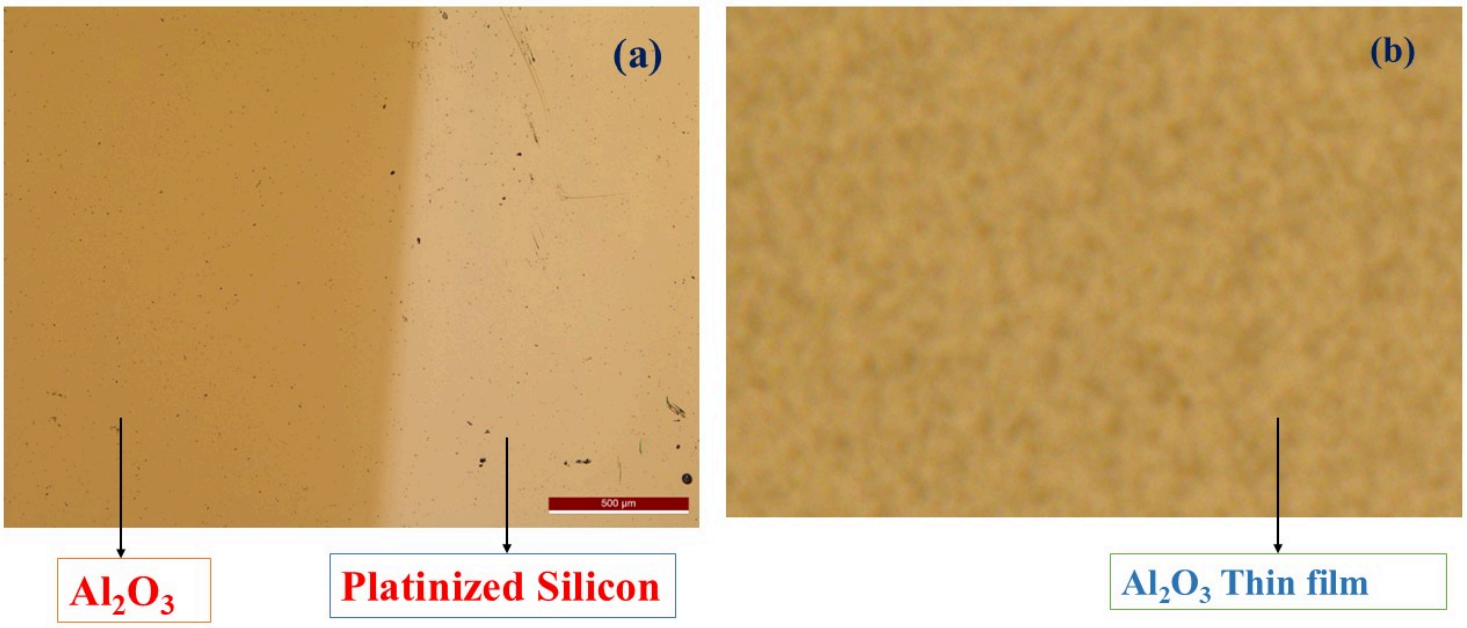


Figure 1

Optical microscopy images of the RF-sputtered Al_2O_3 thin film on platinized silicon: **(a)**overview showing both the Al_2O_3-coated region and the adjacent platinized silicon surface, and **(b)** magnified view of the Al_2O_3-coated area illustrating the surface morphology of the deposited film.

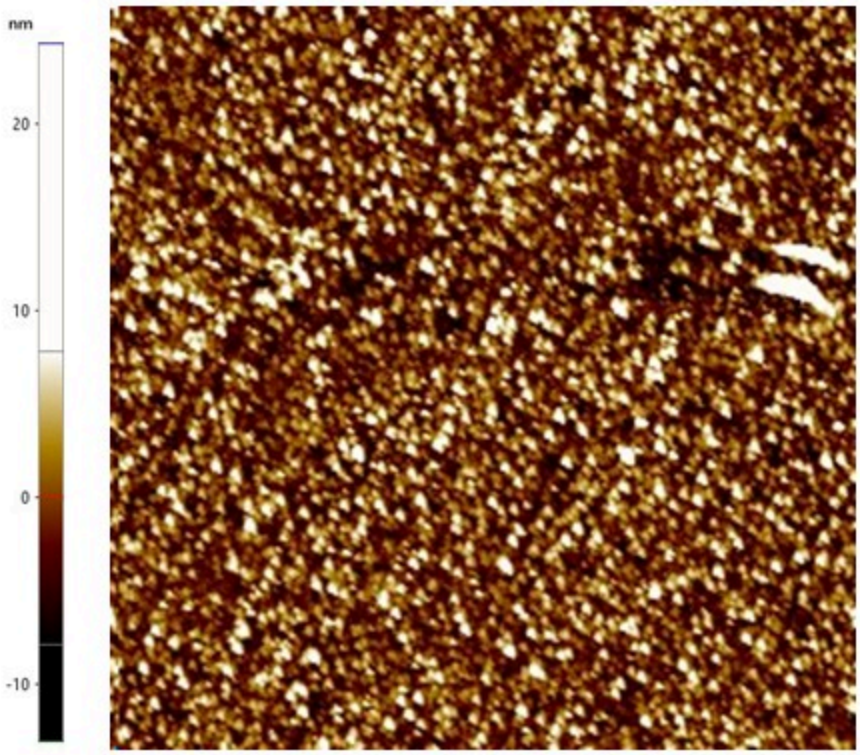


Figure 2

Atomic force microscopy (AFM) topographical image of the RF-sputtered Al_2O_3 thin film deposited on the platinized silicon substrate, illustrating a uniform nanoscale surface morphology. The measured root-mean-square (RMS) surface roughness of the film is approximately 4.006 nm.

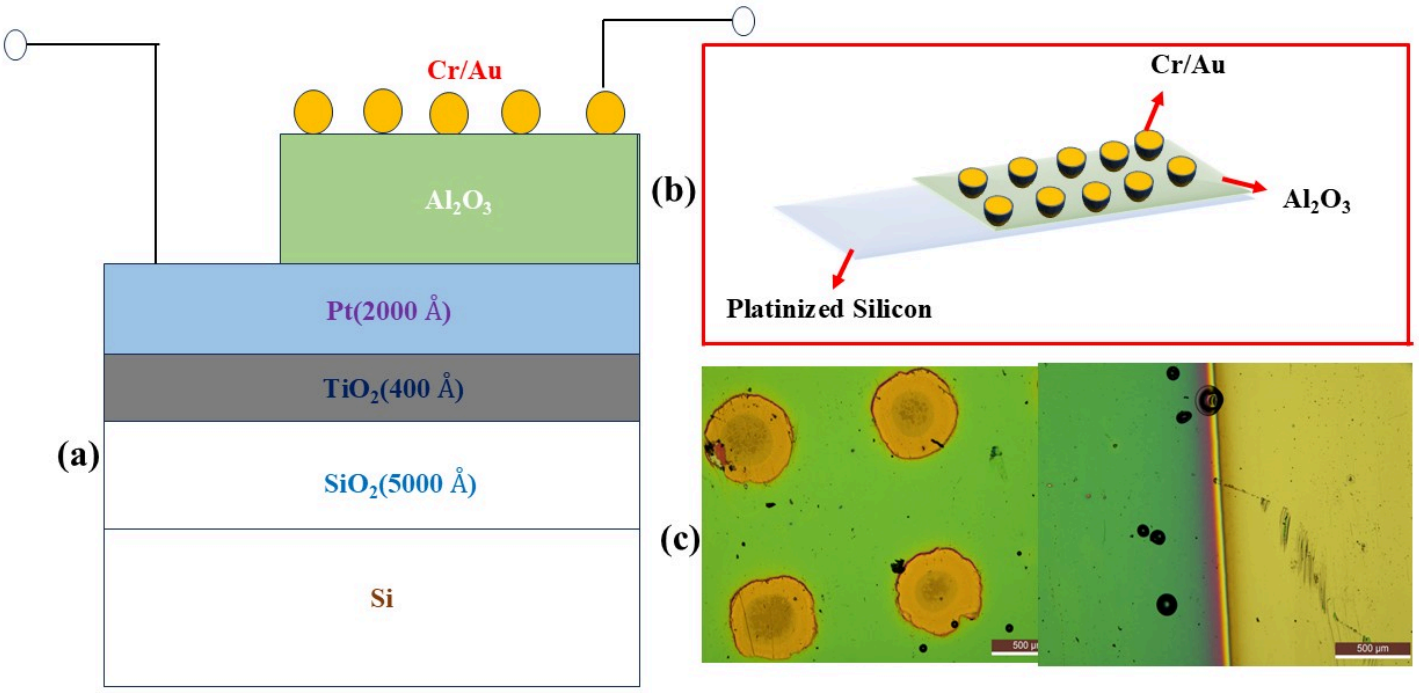


Figure 3

(a) Cross-sectional schematic of the fabricated Pt/Al_2O_3/Cr/Au MIM capacitor on a platinized silicon substrate with electrical connection terminals. **(b)**Schematic top view of the device layout showing the circular top electrodes. **(c)**Optical microscope image of the fabricated MIM capacitor array after Cr/Au electrode deposition.

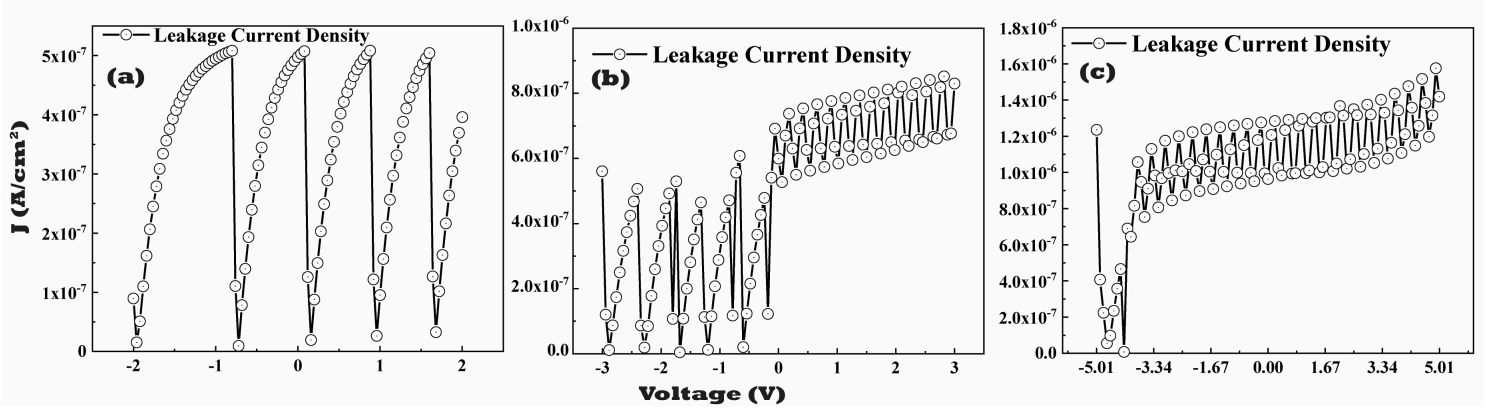


Figure 4

Leakage current density (J) as a function of the applied bias voltage for the fabricated Pt/Al_2O_3/Cr/Au MIM capacitors measured under different voltage sweep ranges: **(a)** −2 V to +2 V, **(b)** −3 V to +3 V, and **(c)** −5 V to +5 V.

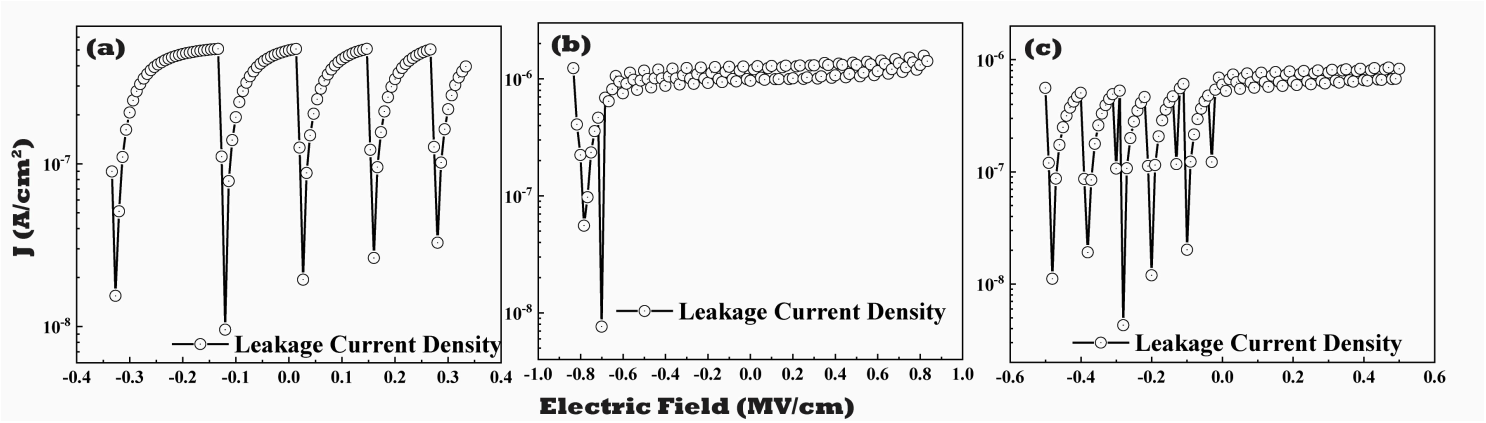


Figure 5

Leakage current density (J) as a function of the applied electric field (E) for the fabricated Pt/Al_2O_3/Cr/Au MIM capacitors under different bias sweep ranges: **(a)** corresponding to −2 V to +2 V, **(b)**corresponding to −3 V to +3 V, and **(c)** corresponding to −5 V to +5 V. The electric field was calculated from the applied voltage and the Al_2O_3 dielectric thickness (60 nm).

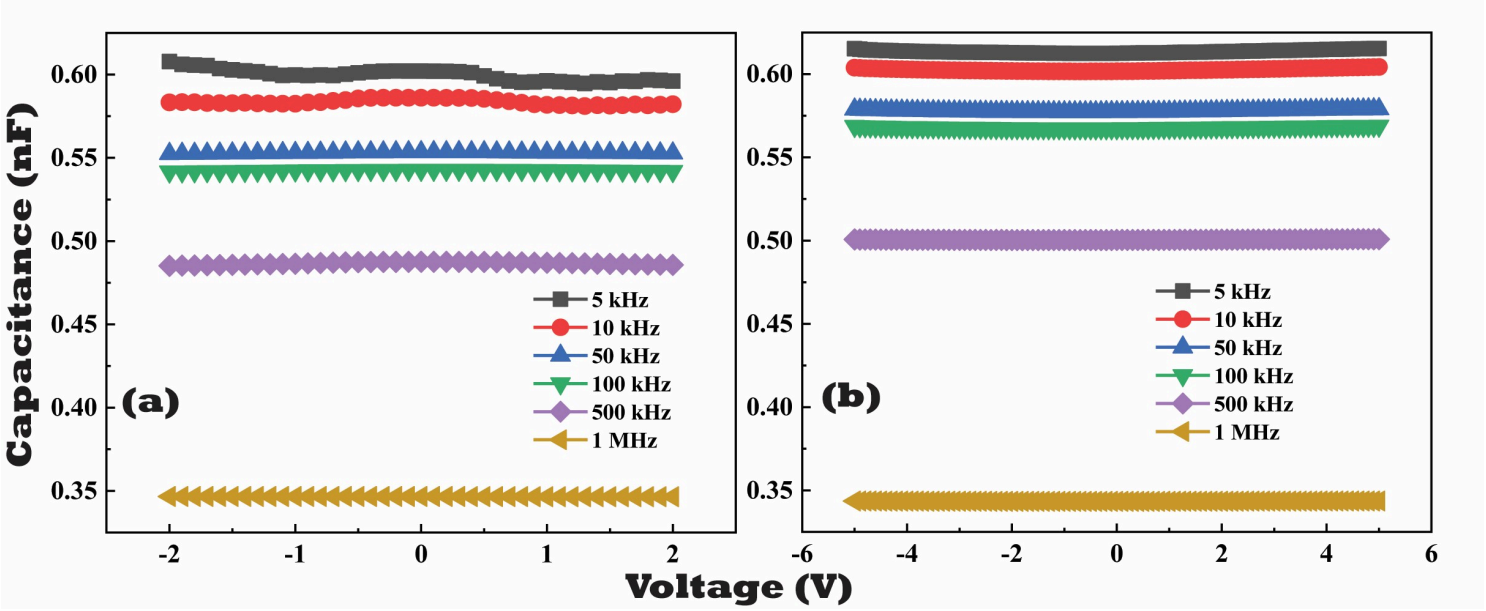


Figure 6

Capacitance–voltage (C–V) characteristics of the fabricated Pt/Al_2O_3/Cr/Au metal–insulator–metal (MIM) capacitors measured at frequencies of 5 kHz, 10 kHz, 50 kHz, 100 kHz, 500 kHz, and 1 MHz under different voltage sweep ranges: **(a)** −2 V to +2 V and **(b)**−5 V to +5 V.

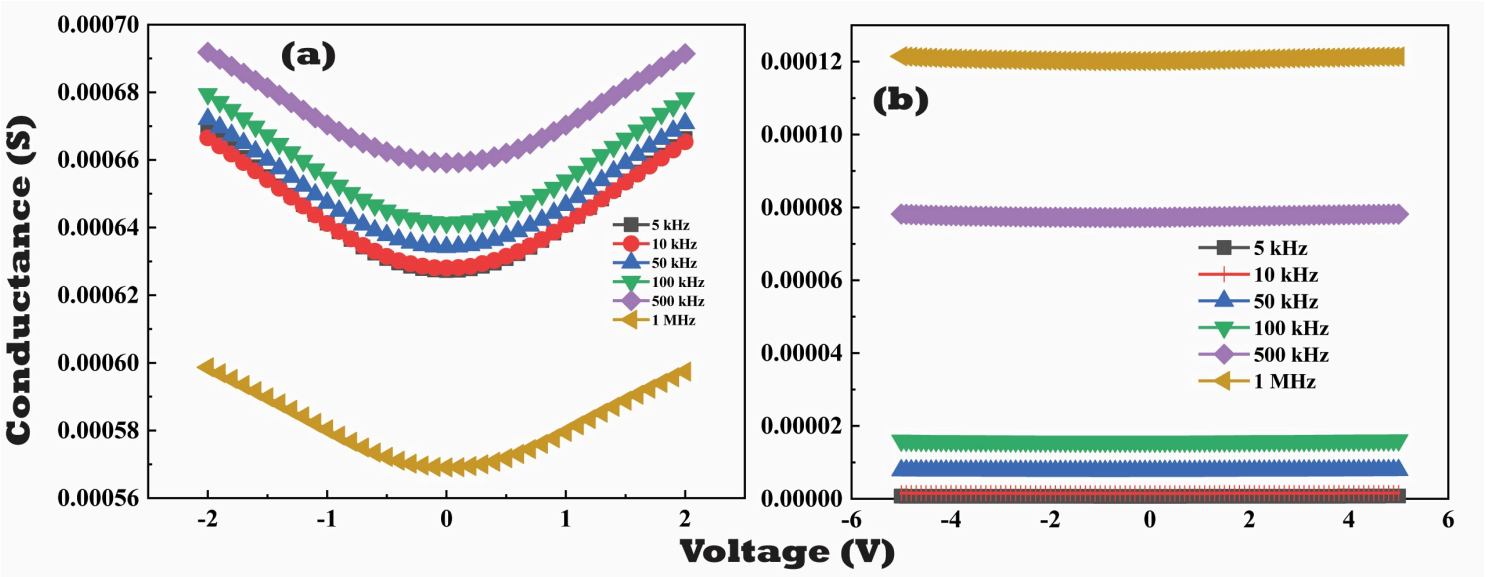


Figure 7

Conductance–voltage (G–V) characteristics of the fabricated Pt/Al_2O_3/Cr/Au metal–insulator–metal (MIM) capacitors measured at frequencies of 5 kHz, 10 kHz, 50 kHz, 100 kHz, 500 kHz, and 1 MHz under different voltage sweep ranges: **(a)** −2 V to +2 V and **(b)**−5 V to +5 V.

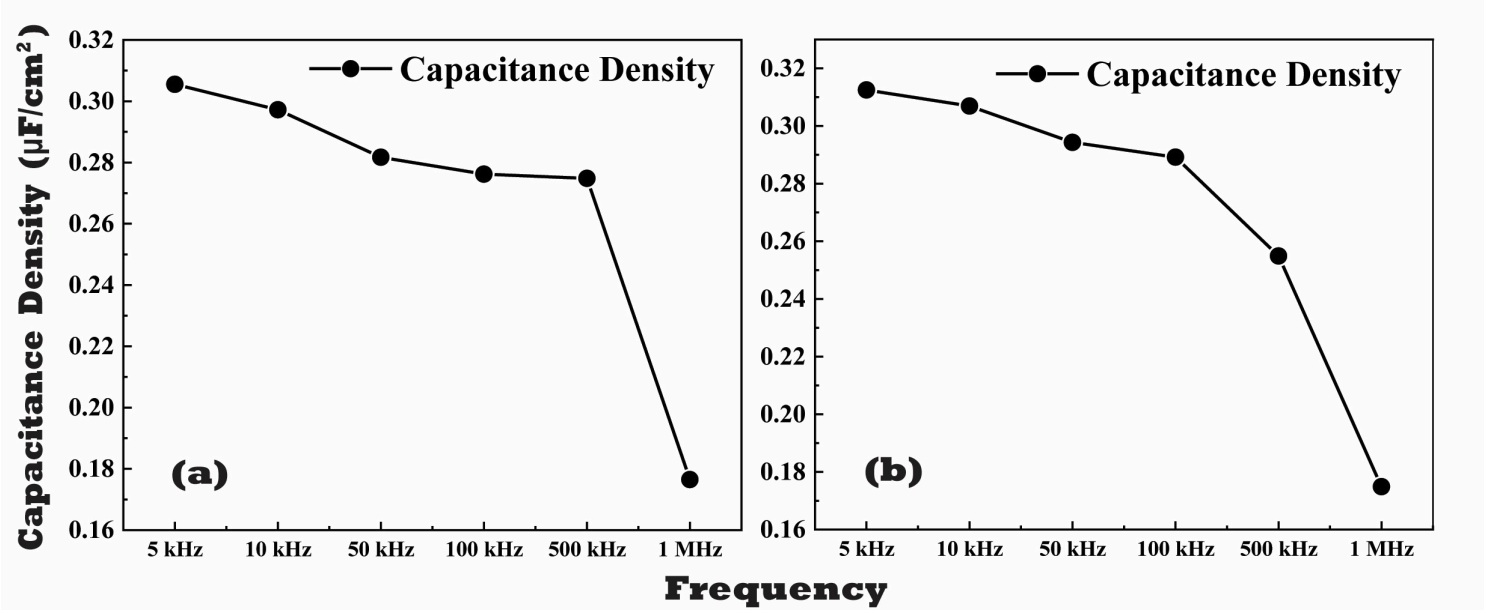


Figure 8

Variation of capacitance density with measurement frequency for the fabricated Pt/Al_2O_3/Cr/Au metal–insulator–metal (MIM) capacitors. The capacitance density was evaluated at frequencies of 5 kHz, 10 kHz, 50 kHz, 100 kHz, 500 kHz, and 1 MHz for voltage sweep ranges of **(a)** −2 V to +2 V and **(b)** −5 V to +5 V.

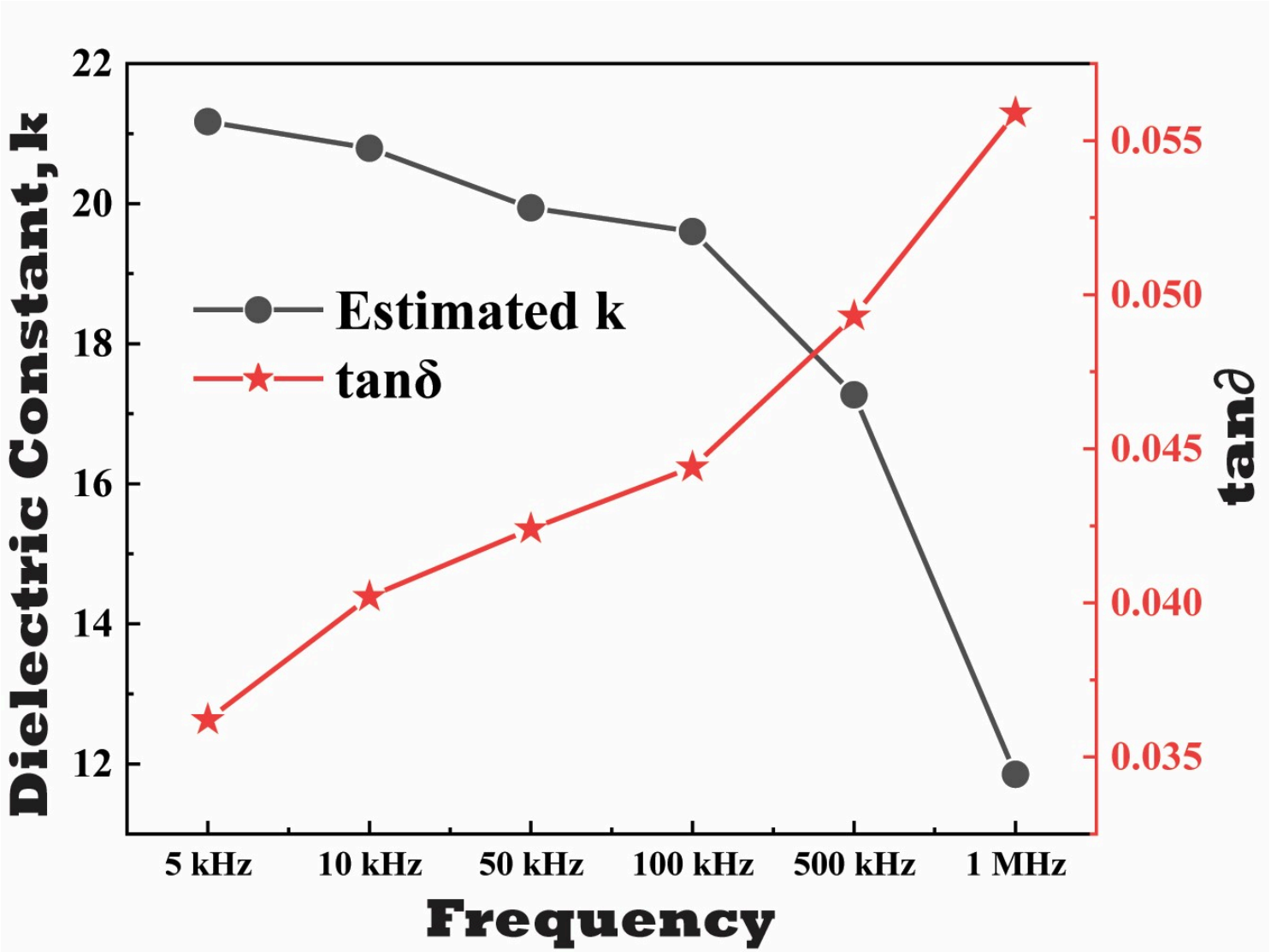


Figure 9

Frequency dependence of the estimated dielectric constant (k) and loss tangent (tanδ) for the fabricated Pt/Al_2O_3/Cr/Au MIM capacitors, extracted from capacitance and conductance measurements obtained over the −5 V to +5 V voltage sweep.

Supplementary Files

This is a list of supplementary files associated with this preprint. Click to download.

- GAMIMAl2O3.jpg